Caveolin-1 and mechanical stress control the release of a pro-metastatic subpopulation of small extracellular vesicles

Cristian Saquel[1,2,3], Celine Gracia[1,2,3], Christine Viaris de Lesegno[1,2,3], Frederik Verweij[4,5], Carlos Urena-Martin[1,2,3,&], Graça Raposo[6], Christophe Lamaze[1, 2, 3,*]

[1] Institut Curie - Centre de Recherche, PSL Research University, Membrane Mechanics and Dynamics of Intracellular Signaling Laboratory, Paris, France.

[2] Institut National de la Santé et de la Recherche Médicale (INSERM), U1143, Paris, France.

[3] Centre National de la Recherche Scientifique (CNRS), UMR 3666, Paris, France.

[4] Department of Cell Biology, Neurobiology and Biophysics, Utrecht University, Utrecht, The Netherlands.

[5] Centre for Living Technologies, Alliance Eindhoven University of Technology, Wageningen University & Research, Utrecht University, University Medical Center Utrecht, The Netherlands.

[6] Institut Curie, PSL Research University, CNRS, UMR144, Structure and Membrane Compartments, 75005 Paris, France.

[&] Current address: esi3N|CENIMAT, Department of Materials Science, NOVA School of Science and Technology, NOVA University Lisbon, Campus de Caparica, 2829-516 Caparica, Portugal.

* Corresponding author: Christophe Lamaze, christophe.lamaze@curie.fr

Abstract

Extracellular vesicles are lipid-enclosed vesicles released by most cells and are present in all human bodily fluids. EVs carry genetic material and proteins, which can be transferred to other cells, generating various biological effects. Caveolin-1 (Cav1) is a key structural protein of the small invaginations of the plasma membrane known as caveolae, which function as mechano-sensors and membrane tension buffering devices. Elevated levels of Cav1 have been detected in EVs from patients with advanced cancer. Given the importance of mechanical forces within the tumor microenvironment, we investigated the potential role of caveolae and Cav1 in regulating EV dynamics and cancer progression under mechanical stress. Our study revealed that different types of mechanical stress significantly induce the release of EVs from several cancer cell lines. These EVs were characterized as exosomes enriched for Cav1. Notably, we found that functional Cav1 was essential for the stress-induced increase in EV production. Lipidomic and proteomic analyses showed differences in the composition of EVs between WT and Cav1-deficient cells and between resting cells and cells subjected to mechanical stress. Additionally, EVs isolated from mechanically stressed cells were shown to promote enhanced migration and invasion of cancer cells in a Cav1-dependent manner. Altogether, our data uncover a new role for Cav1 in mediating cell-to-cell communication and promoting the acquisition of metastatic traits through the mechanical regulation of EV production and dynamics.

Introduction

Extracellular vesicles (EVs) are small membranous particles present in all bodily fluids, released into the extracellular space by all cell types studied thus far (Théry et al., 2018). In recent years, EVs have garnered significant attention due to their involvement in a wide range of physiological and pathological processes, including cancer (Yáñez-Mó et al., 2015). Within the context of cancer, EVs are implicated in multiple aspects of tumor progression and metastasis, such as promoting cell proliferation, invasion, angiogenesis, and immune evasion. Notably, tumor cells release higher amounts of EVs compared to healthy cells. Tumor-derived EVs influence the local tumor microenvironment, can travel to distant secondary sites, and serve as a mode of communication between cancerous and non-cancerous cells, ultimately promoting cancer progression (Chen et al., 2018; Peinado et al., 2012; Sung et al., 2015).

Caveolae are specialized, 60-80 nm cup-shaped invaginations of the plasma membrane found in most cell types (Lamaze et al., 2017; Palade, 1953). The structural and functional integrity of caveolae depends on both caveolins and cavins (Kovtun et al., 2015). Mutations or abnormal expression of caveolae components have been linked to various disorders, including cancer (Le Lay & Kurzchalia, 2005 ; Martinez-Outschoorn, et al., 2015). The caveolae protein caveolin-1 (Cav1) is more abundant in tumor-derived EVs and has been proposed as a biomarker for cancer progression (Campos et al., 2019; Lamaze & Torrino, 2015). In 2011, a new function of caveolae was established as mechano-sensors and mechano-transducers, which are essential for cell mechano-protection (Dewulf et al., 2019; Sinha et al., 2011; Torrino et al., 2018). As tumors progress and metastasize, their physical

microenvironment undergoes significant changes. Throughout the metastatic journey from the primary site to distant secondary locations, tumor cells must continuously adapt and respond to varying mechanical stresses encountered along the way.

In this study, we explored the role of caveolae in EV dynamics in cancer cells subjected to mechanical strain. We observed a significant increase in the release of EVs following mechanical stress. This increase in EV production was dependent on Cav1 and the endosomal sorting complex required for transport (ESCRT)-0 proteins, indicating an exosomal origin. This specific subpopulation of Cav1-positive EVs exhibited a particular lipid and protein signature and was able to induce metastatic traits in recipient cells, including increased migration and invasion *in vitro*. Our findings reveal a novel mechanism by which cancer cells exploit the mechanical properties of caveolae to adapt to the mechanical environment of tumors and promote the secretion of pro-metastatic EVs.

Results

Mechanical stress amplifies the release of small EVs.

To investigate the effect of mechanical stress on the release of small EVs, we first applied a hypo-osmotic shock, in which cells were briefly exposed to a hypo-osmotic medium, causing the flattening of caveolae (Sinha et al., 2011) (**Figure S1A**). EVs were purified from wild-type (WT) HeLa cells under resting or osmotic shock conditions using ultracentrifugation. Nanoparticle tracking analysis (NTA) of the size distribution revealed that most secreted EVs ranged between 50-200 nm (**Figure 1A**). Notably, cells subjected to hypo-osmotic shock exhibited a substantial 3.5-fold increase in secreted EVs, as measured by NTA (**Figure 1B**). To assess the purity

and integrity of the released EVs, we used electron microscopy (EM). EM images showed EVs with the characteristic “donut” shape albeit with a smaller mean diameter (~80 nm) compared to the average size measured by NTA (~128 nm mean size). This discrepancy in EV size is a known artifact of the preparation method used for transmission electron microscopy (TEM) (Wu et al., 2015) (**Figure 1C and 1D**). Western blot analysis confirmed the presence of *bona fide* EV markers, including CD63 and CD9 as previously described (Mathieu et al., 2021). The endoplasmic reticulum (ER) protein calnexin, commonly used as a negative marker, was present in cell extracts but absent in EVs, as expected. Additionally, the two main components of caveolae, Cav1 and cavin1, were detected in the EVs from WT HeLa cells. Notably, both proteins showed an approximate 2.5-fold enrichment in EVs from cells subjected to hypo-osmotic shock compared to those from resting cells (**Figure 1E**).

Cav1 is essential for the enhanced release of small EVs induced by mechanical stress.

Given the role of caveolae in mechano-sensing, we investigated their involvement in the increased release of EVs induced by mechanical stress. Remarkably, in HeLa cells stably knocked out for Cav1 expression, the hypo-osmotic no longer triggered an increase in EV secretion (**Figure 2A**). To ensure this effect was not specific to the two-dimensional hypo-osmotic shock model, we tested a three-dimensional osmotically induced mechanical compression model using multicellular spheroids grown on an agarose bed with high molecular weight dextran (2 MDa), a sugar neutral to mammalian cell metabolism (**Figure S1D and S1E**) (Dolega et al., 2017). We found that this alternative type of mechanical strain also led to the disassembly

of caveolae without affecting cell viability (**Figure S1E-G**). Dextran compression of spheroids induced a significant two-fold increase in the number of secreted EVs detected by NTA, compared to resting spheroids. As with hypo-osmotic shock, the absence of Cav1 prevented this increase in EV secretion (**Figure 2B**). Cavin1 is required for caveolae morphogenesis and stability at the plasma membrane. In the absence of cavin1, caveolae fail to form, and only Cav1 is present at the plasma membrane, albeit at lower expression levels (Drab et al., 2001; Hill et al., 2008). In HeLa cells stably knocked out for cavin1, mechanical stress still caused an increase in EV secretion, though this increase was significantly less pronounced than in WT HeLa cells (**Figure 2A and 2B**). Since cavin1 depletion is known to reduce Cav1 levels due to co-transcriptional regulation (Hill et al., 2008), we re-expressed Cav1 in Cavin1-deficient HeLa cells to restore its basal levels. Under these conditions, EV secretion returned to levels comparable to those induced by mechanical stress in WT HeLa cells (**Figure S2D**). These findings suggest that Cav1, but not the full assembly of caveolae, is required for the increase in EV secretion under mechanical stress.

We extended this mechanism to other cell types, including triple negative breast cancer cell lines Hs578t and MDA-MB-231. In these cells, both hypo-osmotic shock and dextran compression induced an increase in EV release, as detected by NTA. This increase was also dependent on the presence of Cav1 (**Figure S2A-C**).

Different mechanisms could lead to an increase of EV production, including enhanced secretion by producing cells or impaired reuptake. To address the latter possibility, we specifically measured EV release using a CD63-pHluorin reporter-construct as previously described (Verweij et al., 2018). CD63-pHluorin is a pH-sensitive reporter protein that fluoresces once the pH inside endosomal acidic

compartments is neutralized, such as multivesicular bodies (MVB), containing intraluminal vesicles (ILV), the precursors of exosomes. This optical sensor thus allows visualization of MVB fusion at the plasma membrane and the subsequent release of ILVs as exosomes into the (pH-neutral) extracellular medium in live cells. In line with EV secretion results measured by NTA, exosomal release activity in HeLa cells increased following osmotic shock (**Figure 2C**). This increase in fusion activity after mechanical stress was absent in HeLa Cav1$^{-/-}$ cells, confirming that the enhanced EV detection was due to increased EV release by the producing cells. Altogether, these findings reveal a novel Cav1-dependent mechanism by which hypo-osmotic shock and 3D mechanical compression dramatically increase the release of small EVs (i.e. exosomes) from cells.

Mechanical release of small EVs depends on the endosomal ESCRT-0 complex.

We next explored the mechanism by which the MVB pathway is influenced by mechanical stress or Cav1 depletion. First, we used EM to analyze the characteristics of MVBs in Hs578t cell spheroids under resting conditions, as well as after 5 min, 1 day, and 5 days of dextran compression (**Figure 3A**). Although the diameter of MVBs after mechanical compression did not show significant changes over time (**Figure 3B**), the overall number of MVB-like structures in compressed Hs578t spheroids was significantly reduced compared to resting spheroids across all compression durations (**Figure 3C**). Additionally, in HeLa cells subjected to osmotic shock, we observed enlarged CD63-positive endosomal-like structures decorated with Cav1 (**Figure S1B and S2C, inserts**).

We next evaluated the protein levels of components in the ESCRT pathway, a key machinery controlling MVB biogenesis and exosome production. The signal-transducing adaptor molecule (STAM) binds to hepatocyte growth factor-regulated tyrosine kinase substrate (HRS) to form the ESCRT-0 complex at early endosomes (Migliano et al., 2022). Using western blot analysis, we found that both HRS and STAM were significantly downregulated, with their expression reduced to approximately 45% in the absence of Cav1 (**Figure 4A and 4B**). Additionally, the lysosomal marker Lamp1 and the autophagy marker LC3b were upregulated in Cav1-depleted cells, further confirming alterations in the endosomal pathway (**Figure 4A and 4B**). Next, we tested the effect of ESCRT-0 downregulation on the mechanically induced increase in EV release. Treating WT HeLa cells with siRNA targeting HRS led to efficient downregulation of HRS (>90%) and a milder downregulation of STAM (~50%) (**Figure 4C**). We then purified EVs from HRS-downregulated cells subjected to hypo-osmotic shock. NTA revealed a significant reduction in secreted EVs in HeLa cells treated with siRNA against HRS, confirming HRS's established role of in EV biogenesis (Colombo et al., 2013, 2014). Notably, mechanical stress failed to increase the number of secreted EVs in HRS-downregulated HeLa cells, indicating that the mechanically induced EV release also depends on ESCRT-0. This suggests a co-regulation of this effect by both Cav1 and ESCRT-0 (**Figure 4D**).

Mechanically stressed cells release small EVs with a distinct lipid and protein signature.

Caveolae organize lipid nanodomains at the plasma membrane that are enriched in cholesterol and sphingolipids, and they play a central role in regulating lipid

homeostasis (Krishna & Sengupta, 2019; Prakash et al., 2021; Sonnino & Prinetti, 2009). We investigated whether mechanical stress and Cav1 depletion affect the lipid composition of EVs. To this end, we performed lipidomic analysis of EVs purified from WT and Cav1$^{-/-}$ HeLa cells under resting conditions and after exposure to mechanical stress. Mass spectrometry revealed significant differences in the lipid composition of EVs between WT and Cav1-depleted HeLa cells, as well as between EVs derived from resting and mechanically stressed HeLa cells.

Mechanical stress specifically enriched certain lipid species in EVs, including phosphatidylcholine, O-phosphatidylcholine, phosphatidylethanolamine, O-phosphatidylethanolamine, and phosphatidylinositol. In contrast, mechanical stress resulted in a decrease in cholesterol and ceramide content in EVs. Cav1 depletion in cells led to an increase of lactosylceramide (LacCer), alongside a decrease in ceramide and the gangliosides Gb4 and GM2 in EVs (**Figure 5A-C**).

Cav1 has been implicated in the sorting of various proteins into EVs. Recent studies have demonstrated that Cav1-dependent sorting of specific adhesion proteins, such as tenascin-C and fibronectin, into EVs can promote malignancy in recipient cells (Albacete-Albacete et al., 2020; Campos et al., 2018a, 2023). To assess whether mechanical stress alters the protein content of EVs, particularly proteins involved in cell adhesion and ECM organization, we performed proteomics analysis of EVs from WT and Cav1-depleted cells under both mechanical stress and resting conditions. Our analysis revealed notable differences between EVs from cells in resting conditions and mechanically stressed, as well as between WT and Cav1-depleted cells. Qualitative analysis, focusing on proteins enriched with at least three distinct peptides, showed that while the majority of proteins were common across all four conditions, each condition also contained a distinct subset of unique proteins (**Figure**

6A). Principal component analysis (PCA) revealed a clear separation between EVs from WT cells and Cav1-depleted cells. Interestingly, EVs from control and mechanically stressed Cav1-depleted cells clustered closer together (**Figure 6B**).

A volcano plot representing the relative abundance of proteins in EVs from WT cells under control or mechanical stress conditions revealed significant enrichment ($P < 0.05$) of several proteins in EVs released after mechanical stress. Notably, these EVs were enriched in classic EV markers such as CD63, CD9, TSG101, Lamp1 and Flotillin-1. In addition, there was a marked enrichment of caveolar proteins, including Cav1, cavin1, and EHD2 (**Figure 6C**). The presence of several of these EV and caveolar proteins was further validated by western blot analysis (**Figure 6D**). Interestingly, we observed substantial differences in integrin enrichment between EV samples. Most integrins were significantly more abundant in EVs from WT cells after osmotic shock compared to those from WT cells in resting conditions (**Figure 6E**). Furthermore, a comparison of EVs from WT and Cav1-depleted cells under control conditions showed significant decrease ($P < 0.05$) of various proteins associated with ECM remodeling and ECM components, such as collagenases, metalloproteinases, Tenascin-C, fibronectin, collagen, and laminin, among others (**Figure 6F**).

To further analyze the potential signaling pathways down-regulated in EVs from WT or mechanically stressed cells, we performed gene ontology (GO) enrichment analysis using the myProMS software (myproms-demo.curie.fr/). Proteins were classified by biological processes. In agreement with the specific proteins enriched in EVs from WT cells, the analysis revealed that biological processes such as cell adhesion, ECM organization, wound healing, and cell motility were significantly

enhanced in EVs from WT cells compared to those from Cav1-depleted cells (**Figure 6G**).

Mechanically stressed cells release small EVs that enhance cancer cell migration and invasion.

The differences in lipid and protein composition of EVs induced by mechanical stress or Cav1 absence led us to hypothesize that EVs released under mechanical stress could convey distinct functions to recipient cells. To investigate this, we assessed the impact of EV uptake in cancer biology through cell proliferation and invasion assays. Cell proliferation was evaluated using a wound-healing assay (Ilina & Friedl, 2009). We found that EVs from mechanically stressed cells accelerated wound closure in WT Hs578t cells compared to EVs from resting cells (**Figure 7A-C**). Importantly, the presence of Cav1 was essential for this effect, as EVs secreted from Cav1-deleted cells did not promote wound closure under either resting or mechanical stress conditions. We also assessed the invasive potential of these EVs by pre-incubating recipient cells with the EVs for 24 h, and then evaluating their invasiveness through a thin layer of Matrigel, which contains collagen type IV, entactin, heparan sulfate proteoglycan, and laminin. EVs from mechanically stressed cells enhanced the invasion of Hs578t cells through the ECM, whereas EVs from resting cells also increased the invasion, though to a lesser extent. Importantly, EVs from Cav1-deleted cells failed to enhance invasion, indicating that Cav1 is crucial for this effect (**Figure 7D**).

To determine whether differences in EV uptake by recipient cells might account for their pro-migratory and invasive effects, we analyzed the uptake of CFDA-SE-labeled EVs. CFDA-SE is a membrane-permeable dye that fluoresces upon

cleavage by esterases present in the EVs to create CFSE (Morales-Kastresana et al., 2017). To rule out variations in EV uptake from WT and Cav1-depleted HeLa cells as a factor influencing the increased migration and invasion observed in recipient cells, we stained equal numbers of EVs from both conditions with CFSE and assessed their uptake after 4 h. The uptake of EVs from WT and Cav1-depleted cells was comparable in Hs578t cells (**Figure S3A and S3B**).

In summary, our data indicate that EVs secreted by HeLa cells in response to mechanical stress enhance the migratory and invasive capabilities of Hs578t cells through the ECM in a Cav1-dependent manner, thereby increasing their tumorigenic potential. In contrast, EVs from resting HeLa cells do not confer these properties to Hs578t cells.

Discussion

In this study, we investigated EVs whose release is specifically increased after mechanical stress and identified Cav1, the primary constituent of caveolae, as a central player in this process. Our findings show that EVs released from mechanically stressed cancer cells exhibit a distinct lipid and protein signature and promote enhanced *in vitro* migration and invasion. These effects are dependent on the presence of Cav1.

The average size distribution of EVs purified from HeLa WT, Cav1$^{-/-}$, and cavin1$^{-/-}$ cells ranged up to approximately 350 nm, with over 80% being smaller than 200 nm, which falls within the typical exosome size range. We confirmed their exosomal nature by monitoring MVB fusion with the plasma membrane using the pHluorin-

CD63 construct and by demonstrating dependence on a functional ESCRT-0 complex.

In addition to well-established EV markers like CD63 and CD9 (Keerthikumar et al., 2016; Mathieu et al., 2021), we detected Cav1 and cavin1 in EV samples from WT HeLa cells. This is consistent with previous studies reporting Cav1 in EVs from cancer cells (Campos et al., 2018b; Logozzi et al., 2009).

The molecular mechanisms underlying the increase in EV release during mechanical stress remain unclear. We found that both Cav1 and the ESCRT-0 complex are crucial for this mechanically induced increase in EV release. Previous studies have suggested a potential interaction between Cav1 and the ESCRT machinery. Specifically, in HeLa cells, depletion of HRS was found to reduce the ubiquitination-dependent targeting of Cav1 to intraluminal vesicles (ILVs) within MVBs. Additionally, it has been proposed that overexpression of Cav1 leads to its accumulation in endosomal structures (Hayer et al., 2010).

Given the critical role of caveolae in mechano-sensing and mechano-protection, we hypothesized that cancer cell lines with varying levels of Cav1 expression might respond differently to mechanical stress. This is particularly relevant considering the mechanical challenges that cancer cells face as they progress from tumor growth to metastasis (Northcott et al., 2018). Cav1 is known to enhance metastatic traits, such as cell migration, invasion and resistance to anoikis (Díaz et al., 2014; Urra et al., 2012; Wang et al., 2018), although the exact mechanism(s) remain poorly understood. Recently, the presence of Cav1 in EVs from breast cancer cells was associated with increased migration and invasion of epithelial T47-D and TNBC MDA-MB-231 recipient cells (Campos et al., 2018b). Our assessment of the metastatic potential of EVs released from mechanically stressed or resting WT and

Cav1-depleted revealed increased migration and invasion of Hs578t cells when incubated with EVs from HeLa cells. This effect was further enhanced with incubation with EVs secreted under mechanical stress. This effect was depended on the presence of Cav1 in donor cells. Since Hs578t cells already express Cav1, it suggests that the enhanced migratory and invasive effects of EVs may not be solely attributed to the presence of Cav1 within the EVs themselves but could also be linked to changes in the overall composition of the EV subpopulation induced by mechanical stress.

We explored the components of the EVs responsible for these effects, considering Cav1's role in lipid clustering at the plasma membrane and lipid nanodomain assembly (Pohl et al., 2002; Pol et al., 2005), as well as its role in sorting specific proteins into EVs (Albacete-Albacete et al., 2020; Campos et al., 2018, Campos et al., 2023). Mechanical forces can alter lipid distribution in membranes, leading to lipid phase separation in giant unilamellar vesicles (GUV) (Colom et al., 2018). Our lipidomic analyses revealed significant differences in lipid composition between EVs from WT and Cav1-depleted cells, and between resting and mechanically stressed cells. Notably, mechanical stress led to increased incorporation of globoside Gb4 and ganglioside GM2 into EVs from WT cells, with Cav1 depletion preventing this incorporation. Gb4 has been demonstrated to stimulate the Raf-MEK-ERK MAPK signaling pathway, leading to increased cancer cell proliferation (Park et al., 2012). GM2 role in cancer progression is well-documented, as it is highly expressed in various human tumors and functions as a pro-cancer signaling regulator (Sasaki et al., 2021).

Differential protein composition within EVs can significantly influence various aspects of their biology, including organotropism and their effects on recipient cells. Our

proteomic analysis revealed a diverse array of proteins in EVs, which exhibited significant alterations. Consistent with previous findings, we observed an enrichment of adhesion molecules, such as Tenascin-C and fibronectin into Cav1-positive EVs. Notably, mechanical stress further increased the enrichment of Cav1 and other proteins associated with ECM organization. These proteins are known to play crucial roles in cell adhesion and in enhancing the migratory and invasive capabilities of recipient cells, thereby promoting malignancy (Campos et al., 2023; Dourado et al., 2019). Additionally, we detected changes in the enrichment of several integrins in EVs from mechanically stressed cells, suggesting potential modifications in their organotropism, docking, and uptake by recipient cells (Hoshino et al., 2015). Overall, our proteomics data reveal Cav1 and mechanical stress-dependent alterations in EV content that promote pro-metastatic effects, opening new avenues for investigating how these changes may influence cancer progression.

Our findings connect the response of caveolae to mechanical stress with increased EV production. We and others have demonstrated that caveolae flatten to counteract increased membrane tension and prevent rupture under mechanical stress (Sinha et al., 2011). This flattening is followed by disassembly and release of caveolae coat components into the cytoplasm and non-caveolar Cav1 at the plasma membrane. Our results indicate that Cav1, rather than caveolae themselves, is responsible for the increased EV production under mechanical stress, consistent with Cav1's presence in both MVBs and EVs. Under mechanical stress, caveolae flatten and release non-caveolar Cav1, which is subsequently endocytosed into the endosomal network, engulfed into ILVs, and eventually secreted in EVs. Cells lacking Cav1 fail to respond to mechanical stress and do not exhibit increased EV production, while cells lacking cavin1, which possess only non-caveolar Cav1, are still capable of

producing EVs, though at a reduced level. These data strongly suggest a correlation between EV production under mechanical stress and the amount of Cav1 present in MVBs. This was further validated by the increased EV production observed when Cav1 was overexpressed in HeLa cells. Supporting these findings, EM analysis of MVBs revealed a significant enrichment of Cav1 in mechanically stressed cells (**Figure S4**).

In conclusion, our findings underscore the crucial role of Cav1 in regulating EV dynamics in response to the mechanical strains that cancer cells regularly endure. This mechanism offers new insights into how cancer cells can exploit their mechanical environment to enhance cancer progression.

Acknowledgements

The authors greatly acknowledge the Cell and Tissue Imaging (PICT-IBiSA), Institut Curie, member of the French National Research Infrastructure France-BioImaging (ANR10-INBS-04). This work was supported by the Fondation pour la Recherche Médicale (FRM N° DGE20111123020), the Cancerople-IdF (n°2012-2-EML-04-IC-1), InCA (Cancer National Institute, n° 2011-1-LABEL-IC-4), member of the French National Research Infrastructure France-BioImaging (ANR10-INSB-04), and the CurieCoreTech Metabolomics and Lipidomics platform. The authors would like to thank Dr. Clotilde Théry and Dr. Guillaume van Niel for the fruitful discussions and advice during the development of the present work. This work was performed as part of a doctoral thesis supported by grants from Fonds France Canada pour la Recherche (FFCR), Fondation ARC pour la recherche sur le cancer (Grant # ARCDOC42022010004536), and Becas Chile.

Materials and Methods

Cell lines

HeLa, Hs578t, MDA-MB-231 cells along with the Cav1$^{-/-}$ and cavin1$^{-/-}$ sub lines were cultured in Dulbecco's modified Eagle's medium (DMEM-Glutamax, Gibco), with 10% FBS (FBS, Gibco), and 100U/ml penicillin and 100 µg/ml streptomycin (Gibco). Cell lines were grown at 37°C, under 5% CO2. Cell spheroids were prepared following the classical agarose cushion protocol. First, 50 µl of agarose 1,5% w/v in PBS (ultrapure agarose, Invitrogen) and 50 µl per well were dispensed in 96-well plate and incubated for 10-15 min for polymerization at room temperature. Then, cells were seeded on agarose cushion at 105 cells per well. Spheroid formation usually takes between 24 and 48 h. Cav1 and PTRF knockout cells were obtained by CRISPR-Cas9 gene editing.

Antibodies and plasmids

Primary antibodies used include rabbit anti-cav1 (BD Transduction Laboratories, cat. no. 610059; 1:2,000 for WB and 1:200 for IF), mouse anti-Hrs (Abcam, cat. no. ab56468; 1:2,000 for WB), rabbit anti-STAM1/2 (Abcam, cat. no. ab76061; 1:2,500 for WB), mouse anti-CD9 (clone MM2/57; Sigma, cat. no. CBL162; 1:1,000 for WB), mouse anti-α-tubulin (clone B512; Sigma, cat. no. T5168; 1:5,000 for WB), rabbit anti-LC3B (Abcam, cat. no. ab51520; 1:3,000 for WB), mouse anti-CD63 (Santa Cruz, cat. no. sc-5275; 1:2,000 for WB and 1:100 for IF), mouse anti-calnexin (BD transduction laboratories. cat. no. 610523; 1:2,000 for WB), rabbit anti-PTRF (Proteintech. cat. no. 18892-1-ap. 1:1,000 for WB). Secondary antibodies used include mouse-HRP (Jackson ImmunoResearch, cat. no. 715-035-151; 1:5,000 for

WB) and rabbit-HRP (Jackson ImmunoResearch, cat. no. 711-035-152; 1:5,000 for WB), mouse-Alexa 488 (Invitrogen, cat. no. A21202; 1:200 for IF), mouse-Cy3 (Jackson ImmunoResearch, cat. no. 715-166-150; 1:200 for IF), rabbit-Alexa 488 (Invitrogen, cat. no. A21206; 1:200 for IF), rabbit-Cy3 (Jackson ImmunoResearch, cat. no. 111-166-045; 1:200 for IF).

The pCMV-CD63-pHluorin construct (Addgene, #130901) was transfected in HeLa cells using the lipofectamine LTX reagent (Invitrogen) protocol, with 1 µg of plasmid DNA. Cells were imaged 48 h after transfection.

RNA interference

For HRS knockdown we used the following: Control siRNA (Dharmacon, Thermo Fisher, cat. no. SI03650325; 5′-AATTCTCCGAACGTGTCACGT-3′), the Hrs pool of four siRNA SMARTpool ON-TARGETplus HGS siRNA (Thermo Fisher, L-016835-00-0005; 5′-GAGGUAAACGUCCGUAACA-3′, 5′-GCACGUCUUUCCAGAAUUC-3′, 5′-AAAGAACUGUGGCCAGACA-3′ and 5′-GAACCCACACGUCGCCUUG-3′). Transfection was done using Lipofectamine RNAiMAX according to the manufacturer's protocol (Thermo Fisher). siRNA was used at 20 nM. Depletion efficiency was assessed by immunoblotting.

Mechanical stress models

To induce swelling of cells in 2D cultures we used hypo-osmotic shock. Hypo-osmotic shock was performed on cells by using the corresponding growth medium diluted appropriately in deionized water (1:9 dilution for 30 mOsm hypo-osmotic shock).

To induce compression of multicellular spheroids, we used osmotic stress as described by Cappello's team (Dolega et al., 2017). Shortly, we prepared hyperosmotic medium by adding high molecular weight dextran to reach a final concentration of 160 g/ml (2X solution). We used 2 MDa dextran (Sigma Aldrich, 95771) to avoid the penetration of the polymer in the cellular spheroid. Dextran containing medium was added on spheroid at 80 g/ml final concentration. For long-term compression experiments, dextran containing culture medium is renewed after 3 days

EV isolation

For the hypo-osmotic shock experiments, 6×10^6 of cells were seeded per T75 culture flask. After 24 h, cells were washed 1 X with PBS (Gibco) and 12 ml of serum free iso or hypo-osmotic culture medium. Medium was changed after 5 min to iso-osmotic, serum free, culture medium and incubated for the corresponding time periods. For the osmotic induced compression experiments spheroids were washed with 1X PBS (Gibco) and 100 µl of serum free medium containing or not dextran. After treatments with mechanical stimulations (Hypo-osmotic shock or osmotic induced compression) culture supernatant was collected and was subjected to serial centrifugations (2,000 g for 10 min, 11,000 g for 30 min at 4°C), followed by ultracentrifugation at 100,000 g for 90 min at 4°C (45Ti or TLA110 rotors, Beckman Coulter). The pellet containing EVs was washed in cold 1x PBS (Gibco) and ultracentrifuged again at 100,000 g for 90 min at 4°C.

EV characterization by NTA

NTA was performed using ZetaView PMX-120 (Particle Metrix) equipped with a 488 nm laser, with software version 8.05.02 to measure the concentration and distribution size of particles by evaluating the Brownian motion in a light scattering system. The samples were diluted in 1X PBS (Gibco) to obtain a concentration of 10^6 to 10^9 particles/ml per field.

Western blotting

Cell and EV extracts were separated by SDS-PAGE, transferred to nitrocellulose, blocked in 1x PBS containing 3% BSA or 5% nonfat milk according to the antibody used. Membranes were probed overnight at 4°C. Bound antibodies were developed using SuperSignal™ West Femto Maximum Sensitivity Substrate (Thermo Scientific) and the ChemiDoc Touch Imaging System (BioRad). Protein bands were quantified by densitometric analysis using the ImageJ

Electron microscopy

For imaging cell spheroids, epon embedding was used to preserve the integrity of cell structures for electron microscopy (EM). Spheroids were fixed sequentially for 1 h at room temperature with 1.25% glutaraldehyde in 0.1 M Cacodylate and then overnight at 4 °C. Cells were washed extensively with 0.1 M Cacodylate, pH 7.2. Post-fixation was performed for 1 h at room temperature with 1% OsO4 in 0.1 M Cacodylate, pH 7.2. Spheroids were dehydrated through a graded-concentration series of ethanol (50, 70, 90, then 100%, each for 10 min at RT). Embedding was finally performed in LX112 resin. Cells were infiltrated with an increasing ratio of LX112: ethanol solution (1:2, 1:1 and 2:1) and finally with pure LX112. Samples in resin were polymerized overnight at 60°C. Semi-thin 500 nm sections were sliced

using a Leica UCT ultra microtome and mounted onto microscopic glass slides and dried on a hot plate. Semithin sections were stained for 30 s on a hot plate with a mix of Azure B and basic fuchsin in sodium tetraborate (Morikawa et al., 2018). Sections were then mounted in DPX for microscopy and covered with coverslips. Micrographs were acquired on an Upright Wide field Leica DM6000b Microscope equipped with a color CoolSNAP HQ2 camera.

Ultrathin 65 nm sections were sliced using a Leica UCT ultra microtome and mounted on nickel formvar/carbon-coated grids for observations. Contrast was obtained by incubation of the sections for 10 min in 4% uranyl acetate followed by 1 min in lead citrate. Caveolae were identified based on their ultrastructural features. The length of plasma membranes observed were measured using ImageJ software and the number of the structures observed was reported to µm of membrane.

For imaging EVs: EVs pellets were resuspended in 50-100 µl of 1x PBS, 5 µl were deposited on a coated-side of a formvar-carbon grid and left for 20 min to adhere. Grids were then transferred on 2% PFA droplets for 20 mins fixation and then washed 10 times on filtered distilled water droplets. Grids were incubated for 10 mins in 0.4 % uranyl acetate in 2 % methylcellulose droplets on ice and in the dark. Grids were removed from the droplet with a stainless steel loop and excess liquid was removed by pushing the loop on a Whatman filter. Grids are then air dried for 30 mins on the loops.

Electron micrographs were acquired on a Tecnai Spirit electron microscope (FEI, Eindhoven, The Netherlands) equipped with a 4k CCD camera (EMSIS GmbH, Münster, Germany).

Immunofluorescence

After the treatments, cells were fixed with 4% paraformaldehyde (PFA) (EMS) for 15 min at room temperature. Cells were incubated for 1h in a blocking solution: 1x PBS with 0.1% triton and 0.3% BSA. Then primary and secondary antibodies were successively incubated during 1 h each at RT in 1x PBS containing 0.1% triton and 0.1% BSA. Coverslips were then mounted on microscope slides with Fluoromount G (Invitrogen). Images were acquired on a Zeiss LSM 780 confocal microscope with a 63x/1.46 Oil objective. At least 10 cells per replicate were imaged.

Live TIRF microscopy

Cells were grown in 35-mm imaging plates (FluoroDish WPI; IBIDI). An inverted Eclipse Ti-E (Nikon) full motorized with PFS 2 (Perfect Focus System) to reduce the drift was used with a 100 ×CFI PlanApoTIRF, oil, 1.49/0.12-mm objective (Nikon), images were acquired with Metamorph (Molecular Devices). A cage incubator (Life Imaging Services) was used to keep the imaging chamber at 37°C and 5% CO_2. To visualize fusion events, 1-3 min videos were acquired in different areas to analyze at least 20 cells per condition.

Sample preparation for lipidomics

After EV purification by ultracentrifugation, the EV pellet was reconstituted in 200 µl of 150 mM ammonium bicarbonate (NH_4HCO_3), then quickly frozen with liquid nitrogen and stored at -80 °C or later use. Lipids were extracted in chloroform and methanol pre-mixed with internal standard mix, then analyzed at the CurieCoreTech Metabolomics and Lipidomics platform.

EV collection for proteomics

$2,5x10^6$ cells per 10 cm dish were plated the day before the osmotic shock. For each osmotic experiment, medium was collected from 10 plates, while for resting cells, medium from 15 plates. The medium was centrifuged at 2,000g for 15 min, and EVs were purified by ultracentrifugation, following established protocols. The concentration of recovered EVs was measured by nanoparticle tracking analysis (ZetaView, Particle Metrix) and resuspended to a final concentration of $1x10^{11}$ particles in 10 µl of PBS. Four independent biological replicates were analyzed by mass spectrometry, which was performed at the CurieCoreTech Mass Spectrometry Proteomics platform at the Institut Curie.

Migration and invasion assays

Migration assays of Hs578t cells were performed by seeding 300,000 cells in each well of a 24-well plate 24 h before the experiment. The cells were incubated with 1 µg/ml of EVs 37 °C for 4 h. After incubation, a scratch was done in the middle of each well with a pipette tip, cells were washed 1 time with PBS and incubated with FBS-free culture medium. Cell migration was monitored using time-lapse microscopy (IncuCyte Live Cell Analysis Systems, 4x objective lens, Sartorius) with an interval of 3 h during 21 h. Image analysis was performed with ImageJ using a wound healing size tool (Suarez-Arnedo et al., 2020).

Invasion assays were performed in 8 µm pore size 24-well inserts (Greiner bio-one) pretreated with Matrigel (BD Biosciences) according to the manufacturer's instructions. Briefly, the inserts were coated with Matrigel and were left in a 37°C incubator for 30 mins before seeding. Then, 300,000 Hs578t cells previously treated with 1 µg/ml of EVs during 24 h were resuspended in serum-free medium and added to the top of each chamber insert, and medium with FBS as a chemo-attractant was

added to the bottom chamber. After 24 h, inserts were removed, washed and cells that migrated to the lower side of the inserts were stained with 0.1% toluidine blue, washed, and counted in an inverted microscope.

CFSE staining of EVs and uptake

EVs isolated by ultracentrifugation were labeled by incubation with 20 µM CFDA-SE (Thermofisher) for 2 h at 37°C. To eliminate surplus dye, size-exclusion chromatography (SEC) was performed using Exo-spin mini columns (Interchim). CFSE-labeled EVs were then collected, and their particle concentration and fluorescence intensity were analyzed using Nanoparticle Tracking Analysis (NTA) and Nano Flow Cytometry (NanoFCM).

For the uptake experiments, acceptor cells were seeded 24 h before at a density of 100,000 cells per well in a 24-well plate on coverslips. The acceptor cells were then incubated with CFSE-labeled EVs at a final concentration of $5x10^9$ EVs/mL for 4 h at 37 °C. After incubation, the cells were washed with PBS and fixed with PBS 4% paraformaldehyde in PBS for 15 mins at room temperature. The cells were then permeabilized for 30 mins at room temperature in PBS containing 1% bovine serum albumin (BSA) 0.1% Triton-X-100. Cells were stained with WGA-rhodamine (ThermoFischer) for membrane visualization. Image analysis and colocalization quantification were performed using ImageJ software (NIH, Maryland, USA).

Statistical analysis

All analyses were performed using GraphPad Prism version 6.0 to 8.0, (GraphPad Software). Two-tailed (paired or unpaired) Student's t-tests were used when comparing only two conditions. For more than two conditions, the Kruskal–Wallis

test, ordinary one-way ANOVA or two-way ANOVA were used. Significantly different comparisons of means are marked on the graphs with asterisks. Error bars denote SEM or SD.

Figures Legends

Figure 1: Characterization of EVs from mechanically stressed cells.

A. Concentration (particles/ml) and size (nm) of EVs from WT HeLa cells in response to hypo-osmotic shock analyzed by NTA. **B.** Quantification of EVs released from WT HeLa cells in response to hypo-osmotic shock. Graph shows number of total secreted EVs as analyzed by NTA **C.** Vesicle concentration and size of EVs from WT HeLa cells in response to hypo-osmotic shock analyzed by EM. **D.** Representative EM images showing EVs isolated from WT HeLa cells in resting conditions or after hypo-osmotic shock. Scale bar 150 nm. **E.** Western Blot analysis of CD63, CD9, calnexin, Cav1 and cavin1 of WT, Cav1$^{-/-}$ or cavin1$^{-/-}$ HeLa cell lysates and their corresponding purified EVs. Red arrow indicates cavin1. Gels were loaded with EVs from the same number of secreting cells. ***: $P < 0.01$.

Figure 2: Effects of mechanical stress on EV release.

A. Quantification of EVs released by WT, Cav1$^{-/-}$ and cavin1$^{-/-}$ HeLa cells in response to hypo-osmotic shock. Graph shows the number of total secreted EVs quantified by NTA. **B.** Quantification of EVs released by WT, Cav1$^{-/-}$ and cavin1$^{-/-}$ HeLa cells in response to dextran compression. Graph shows the number of total secreted EVs. **C.** Quantification of MVB fusion activity (events per cell and time) of WT or Cav1$^{-/-}$ HeLa cells in response to hypo-osmotic shock. **** $P < 0.0001$, ** $P < 0.01$.

Figure 3: Impact of mechanical stress on multivesicular bodies.

A. Upper panel, representative image of an Hs578t cell spheroid. Scale bar 50 µm. Lower panel, representative EM image of an MVB in an Hs578t cell spheroid. Scale bar 10 nm. **B.** Quantification of MVB diameter in Hs578t cell spheroids after 5 min, 1 day or 5 days of dextran compression. **C.** Quantification of the number of MVBs in Hs578t cell spheroid after 5 min, 1 day or 5 days of dextran compression, represented by area. *** $P < 0.0001$.

Figure 4: Analysis of the ESCRT pathway in EV release.

A. Western Blot analysis of HRS, STAM, Lamp1 and LC3B in WT or Cav1$^{-/-}$ HeLa cells lysates. **B.** Protein signal quantification graphs normalized to the stain free gel. **C.** Cell lysate Western Blot analysis of HRS, STAM, Cav1 and tubulin in HeLa cells treated with siRNA control or siRNA against HRS. **D.** Quantification of EVs released by HeLa cells treated with siRNA control or siRNA against HRS in resting conditions or after mechanical stress. Graph shows the number of total secreted EVs quantified by NTA. *** $P < 0.001$, ** $P < 0.01$.

Figure 5: Lipid signature of EVs from mechanically stressed cells.

A. Mol percentile of each lipid class in EVs from WT or Cav1$^{-/-}$ HeLa cells in resting conditions or after osmotic shock. **B.** Mol percentile of each lipid class in lysates from WT or Cav1$^{-/-}$ HeLa cells in resting conditions or after osmotic shock. **C.** Comparison of the fold change in lipid classes between EVs from WT or Cav1$^{-/-}$ HeLa cells in resting conditions or after hypo-osmotic shock. ** $P < 0.01$, * $P < 0.05$.

Figure 6: Protein signature of EVs from mechanically stressed cells.

A. Venn diagram illustrating the quantitative distribution of proteins identified qualitatively in each fraction by at least three peptides across one of the five biological replicates. **B.** PCA analysis showing the quantitative comparison and separation of fractions. **C.** Volcano plot displaying the quantitative analysis of proteins in WT control compared to WT hypo. The horizontal red line indicates a *P* value of 0.05, and the vertical green lines indicate an absolute fold-change of 1.5. Proteins highlighted are selected as potential specific markers of interest. **D.** Western blot validation of the highlighted proteins of interest from panel C. **E.** Ratio of enrichment of integrins in WT control compared to WT hypo EVs. **F.** Volcano plot showing the quantitative analysis of proteins in WT control compared to Cav1 KO. The horizontal red line indicates a *P* value of 0.05, and the vertical green lines indicate an absolute fold-change of 1.5. Highlighted proteins are selected as potential specific markers of interest. **G.** Quantitative Gene Ontology (GO) term enrichment analysis performed using *my*ProMS Software for WT control versus Cav1 KO control fractions. The top 10 significantly enriched GO categories under Biological Processes are indicated.

Figure 7: Migration and invasion of Hs578t cells treated with EVs.

A. Representative images of wound healing assays on Hs578t cells pre-treated with HeLa EVs from WT or Cav1$^{-/-}$ cells in resting conditions or after exposure to mechanical stress. **B.** Wound closure quantification represented in percentage over time. **C.** Quantification of the slope of the wound closure curves. **D.** Quantification of invasive Hs578t cells pre-treated with HeLa EVs from WT or Cav1$^{-/-}$ cells in resting conditions or after exposure to mechanical stress. ** $P < 0.01$.

Supplementary figure 1: Validation of mechanical stress models.

A. Schematic representation of the effect of hypo-osmotic shock on caveolae. In resting conditions, caveolae are fully budded invaginations where Cav1 and cavin1 can interact. Upon hypo-osmotic shock, caveolae flatten out, resulting in the diffusion of non-caveolar Cav1 at the plasma membrane and loss of interaction between Cav1 and Cavin1. This process is reverted upon return to resting conditions **B.** Representative immunofluorescence of Cav1 and CD63 in HeLa cells in resting conditions and after exposure to hypo-osmotic shock. Bar = 5 μm. **C.** Magnified inserts from B showing enlarged endosome-like structures in the cell after osmotic shock. Bar = 1 μm. **D.** Schematic representation of the dextran compression model on spheroids. Cells are seeded on an agarose bed and left to spontaneously form spheroids. High molecular weight dextran is used to induce osmotic induced mechanical compression of the spheroids. **E.** Representative images of Hs578t spheroids at resting conditions and after 5 min, 1 day and 5 days of mechanical compression. **F.** Representative EM images of caveolae structures (*) observed on spheroids. **G.** Quantification of caveolar structures in Hs578t spheroids at resting conditions and after 5 min, 1 day and 5 days of mechanical compression. Graph represents the data in caveolae per area. * $P < 0.05$.

Supplementary figure 2: Effect of mechanical stress on EV secretion in additional cell lines.

A. Quantification of EVs released by WT, Cav1$^{-/-}$ and cavin1$^{-/-}$ Hs578t cells after exposure to hypo-osmotic shock. Graph shows total secreted EVs. **B.** Quantification of EVs released by WT, Cav1$^{-/-}$ and cavin1$^{-/-}$ Hs578t cells after dextran compression.

Graph shows total secreted EVs. **C.** Quantification of EVs released by WT, Cav1$^{-/-}$ and cavin1$^{-/-}$ MDA-MB-231 cells after exposure to hypo-osmotic shock. Graph shows total secreted EVs. **D.** Quantification of EVs released by WT, cavin1$^{-/-}$, and cavin1$^{-/-}$ overexpressing Cav1 HeLa cells after exposure to hypo-osmotic shock. Graph shows total secreted EVs. ** $P < 0.01$, * $P < 0.05$.

Supplementary figure 3: CFSE-EV uptake by Hs578t cells.

A. Representative confocal images of Hs578t acceptor cells after a 4 h incubation with CFSE-labeled EVs. Bar = 5 μm. **B.** Quantification of CFSE-positive dots per cell in WGA-labeled Hs578t WT cells after a 4 h incubation with CFSE- EVs from WT or Cav1-depleted HeLa cells. Each dot represents the number of CFSE-positive dots per micron, with $n = 24$. Error bars represent error.

Supplementary figure 4: Cav1 localization at MVBs after mechanical stress.

A. Representative EM image of an MVB in MLEC cell in resting conditions. **B.** Representative EM image of an MVB in MLEC cell during hypo-osmotic shock. Immunogold labeling against Cav1. Arrows indicate MVB structures. Scale bar 100 nm.

References

Albacete-Albacete, L., Navarro-Lérida, I., López, J. A., Martín-Padura, I., Astudillo, A. M., Ferrarini, A., Van-Der-Heyden, M., Balsinde, J., Orend, G., Vázquez, J., & del Pozo, M. Á. (2020). ECM deposition is driven by caveolin-1–dependent

regulation of exosomal biogenesis and cargo sorting. *Journal of Cell Biology*, *219*(11). https://doi.org/10.1083/JCB.202006178

Campos, A., Burgos-Ravanal, R., González, M. F., Huilcaman, R., González, L. L., & Quest, A. F. G. (2019). Cell intrinsic and extrinsic mechanisms of caveolin-1-enhanced metastasis. In *Biomolecules* (Vol. 9, Issue 8). https://doi.org/10.3390/biom9080314

Campos, A., Burgos-Ravanal, R., Lobos-González, L., Huilcamán, R., González, M. F., Díaz, J., Verschae, A. C., Acevedo, J. P., Carrasco, M., Sepúlveda, F., Jeldes, E., Varas-Godoy, M., Leyton, L., & Quest, A. F. G. (2023). Caveolin-1-dependent tenascin C inclusion in extracellular vesicles is required to promote breast cancer cell malignancy. *Nanomedicine*, *18*(23), 1651–1668. https://doi.org/10.2217/nnm-2023-0143

Campos, A., Salomon, C., Bustos, R., Díaz, J., Martínez, S., Silva, V., Reyes, C., Díaz-Valdivia, N., Varas-Godoy, M., Lobos-González, L., & Quest, A. F. (2018a). Caveolin-1-containing extracellular vesicles transport adhesion proteins and promote malignancy in breast cancer cell lines. *Nanomedicine*, *13*(20), 2597–2609. https://doi.org/10.2217/nnm-2018-0094

Campos, A., Salomon, C., Bustos, R., Díaz, J., Martínez, S., Silva, V., Reyes, C., Díaz-Valdivia, N., Varas-Godoy, M., Lobos-González, L., & Quest, A. F. (2018b). Caveolin-1-containing extracellular vesicles transport adhesion proteins and promote malignancy in breast cancer cell lines. *Nanomedicine*, *13*(20), 2597–2609. https://doi.org/10.2217/nnm-2018-0094

Chen, G., Huang, A. C., Zhang, W., Zhang, G., Wu, M., Xu, W., Yu, Z., Yang, J., Wang, B., Sun, H., Xia, H., Man, Q., Zhong, W., Antelo, L. F., Wu, B., Xiong, X., Liu, X., Guan, L., Li, T., … Guo, W. (2018). Exosomal PD-L1 contributes to

immunosuppression and is associated with anti-PD-1 response. *Nature*, *560*(7718), 382–386. https://doi.org/10.1038/s41586-018-0392-8

Colom, A., Derivery, E., Soleimanpour, S., Tomba, C., Molin, M. D., Sakai, N., González-Gaitán, M., Matile, S., & Roux, A. (2018). A fluorescent membrane tension probe. *Nature Chemistry*, *10*(11), 1118–1125. https://doi.org/10.1038/s41557-018-0127-3

Colombo, M., Moita, C., Van Niel, G., Kowal, J., Vigneron, J., Benaroch, P., Manel, N., Moita, L. F., Théry, C., & Raposo, G. (2013). Analysis of ESCRT functions in exosome biogenesis, composition and secretion highlights the heterogeneity of extracellular vesicles. *Journal of Cell Science*, *126*(24), 5553–5565. https://doi.org/10.1242/jcs.128868

Colombo, M., Raposo, G., & Théry, C. (2014). Biogenesis, secretion, and intercellular interactions of exosomes and other extracellular vesicles. *Annual Review of Cell and Developmental Biology*, *30*, 255–289. https://doi.org/10.1146/annurev-cellbio-101512-122326

Dewulf, M., Köster, D. V., Sinha, B., Lesegno, C. V. De, Chambon, V., Bigot, A., Bensalah, M., Negroni, E., Tardif, N., Podkalicka, J., Johannes, L., Nassoy, P., Butler-browne, G., Lamaze, C., & Blouin, C. M. (2019). Dystrophy-associated caveolin-3 mutations reveal that caveolae couple IL6/STAT3 signaling with mechanosensing in human muscle cells. *Nature Communications*, 1–13. https://doi.org/10.1038/s41467-019-09405-5

Díaz, J., Mendoza, P., Ortiz, R., Díaz, N., Leyton, L., Stupack, D., Quest, A. F. G., & Torres, V. A. (2014). Rab5 is required in metastatic cancer cells for Caveolin-1-enhanced Rac1 activation, migration and invasion. *Journal of Cell Science*, *127*(Pt 11), 2401–2406. https://doi.org/10.1242/jcs.141689

Dolega, M. E., Delarue, M., Ingremeau, F., Prost, J., Delon, A., & Cappello, G. (2017). Cell-like pressure sensors reveal increase of mechanical stress towards the core of multicellular spheroids under compression. *Nature Communications*, *8*, 14056. https://doi.org/10.1038/ncomms14056

Dourado, M. R., Korvala, J., Åström, P., De Oliveira, C. E., Cervigne, N. K., Mofatto, L. S., Campanella Bastos, D., Pereira Messetti, A. C., Graner, E., Paes Leme, A. F., Coletta, R. D., & Salo, T. (2019). Extracellular vesicles derived from cancer-associated fibroblasts induce the migration and invasion of oral squamous cell carcinoma. *Journal of Extracellular Vesicles*, *8*(1). https://doi.org/10.1080/20013078.2019.1578525

Drab, M., Verkade, P., Elger, M., Kasper, M., Lohn, M., Lauterbach, B., Menne, J., Lindschau, C., Mende, F., Luft, F. C., Schedl, A., Haller, H., & Kurzchalia, T. V. (2001). Loss of caveolae, vascular dysfunction, and pulmonary defects in caveolin-1 gene-disrupted mice. *Science (New York, N.Y.)*, *293*(5539), 2449–2452. https://doi.org/10.1126/science.1062688

Hayer, A., Stoeber, M., Bissig, C., & Helenius, A. (2010). Biogenesis of caveolae: Stepwise assembly of large caveolin and cavin complexes. *Traffic*, *11*(3), 361–382. https://doi.org/10.1111/j.1600-0854.2009.01023.x

Hill, M. M., Bastiani, M., Luetterforst, R., Kirkham, M., Kirkham, A., Nixon, S. J., Walser, P., Abankwa, D., Oorschot, V. M. J., Martin, S., Hancock, J. F., & Parton, R. G. (2008). PTRF-Cavin, a conserved cytoplasmic protein required for caveola formation and function. *Cell*, *132*(1), 113–124. https://doi.org/10.1016/j.cell.2007.11.042

Hoshino, A., Costa-silva, B., Shen, T., Rodrigues, G., Hashimoto, A., Mark, M. T., Molina, H., Kohsaka, S., Giannatale, A. Di, Ceder, S., Singh, S., Williams, C.,

Soplop, N., Uryu, K., Pharmer, L., King, T., Bojmar, L., Davies, A. E., Ararso, Y., … Wexler, L. H. (2015). Tumour exosome integrins determine organotropic metastasis. *Nature*, *527*(7578), 329–335. https://doi.org/10.1038/nature15756

Ilina, O., & Friedl, P. (2009). Mechanisms of collective cell migration at a glance. *Journal of Cell Science*, *122*(Pt 18), 3203–3208. https://doi.org/10.1242/jcs.036525

Keerthikumar, S., Chisanga, D., Ariyaratne, D., Al Saffar, H., Anand, S., Zhao, K., Samuel, M., Pathan, M., Jois, M., Chilamkurti, N., Gangoda, L., & Mathivanan, S. (2016). ExoCarta: A Web-Based Compendium of Exosomal Cargo. *Journal of Molecular Biology*, *428*(4), 688–692. https://doi.org/10.1016/j.jmb.2015.09.019

Kovtun, O., Tillu, V. A., Ariotti, N., Parton, R. G., & Collins, B. M. (2015). Cavin family proteins and the assembly of caveolae. *Journal of Cell Science*, *128*(7), 1269–1278. https://doi.org/10.1242/jcs.167866

Krishna, A., & Sengupta, D. (2019). Interplay between Membrane Curvature and Cholesterol□: Role of Palmitoylated Caveolin-1. *Biophysj*, *116*(1), 69–78. https://doi.org/10.1016/j.bpj.2018.11.3127

Lamaze, C., Tardif, N., Dewulf, M., Vassilopoulos, S., & Blouin, C. M. (2017). The caveolae dress code: structure and signaling. *Current Opinion in Cell Biology*, *47*, 117–125. https://doi.org/10.1016/j.ceb.2017.02.014

Lamaze, C., & Torrino, S. (2015). Caveolae and cancer: A new mechanical perspective. *Biomedical Journal*, *38*(5), 367–379. https://doi.org/10.4103/2319-4170.164229

Le Lay, S., & Kurzchalia, T. V. (2005). Getting rid of caveolins: phenotypes of caveolin-deficient animals. *Biochimica et Biophysica Acta*, *1746*(3), 322–333. https://doi.org/10.1016/j.bbamcr.2005.06.001

Logozzi, M., De Milito, A., Lugini, L., Borghi, M., Calabrò, L., Spada, M., Perdicchio, M., Marino, M. L., Federici, C., Iessi, E., Brambilla, D., Venturi, G., Lozupone, F., Santinami, M., Huber, V., Maio, M., Rivoltini, L., & Fais, S. (2009). High levels of exosomes expressing CD63 and caveolin-1 in plasma of melanoma patients. *PLoS ONE*, *4*(4). https://doi.org/10.1371/journal.pone.0005219

Martinez-Outschoorn, U. E., Sotgia, F., & Lisanti, M. P. (2015). Caveolae and signalling in cancer. In *Nature Reviews Cancer* (Vol. 15, Issue 4, pp. 225–237). Nature Publishing Group. https://doi.org/10.1038/nrc3915

Mathieu, M., Névo, N., Jouve, M., Valenzuela, J. I., Maurin, M., Verweij, F. J., Palmulli, R., Lankar, D., Dingli, F., Loew, D., Rubinstein, E., Boncompain, G., Perez, F., & Théry, C. (2021). Specificities of exosome versus small ectosome secretion revealed by live intracellular tracking of CD63 and CD9. *Nature Communications*, *12*(1), 4389. https://doi.org/10.1038/s41467-021-24384-2

Migliano, S. M., Wenzel, E. M., & Stenmark, H. (2022). Biophysical and molecular mechanisms of ESCRT functions, and their implications for disease. *Current Opinion in Cell Biology*, *75*, 102062. https://doi.org/10.1016/j.ceb.2022.01.007

Morales-Kastresana, A., Telford, B., Musich, T. A., McKinnon, K., Clayborne, C., Braig, Z., Rosner, A., Demberg, T., Watson, D. C., Karpova, T. S., Freeman, G. J., Dekruyff, R. H., Pavlakis, G. N., Terabe, M., Robert-Guroff, M., Berzofsky, J. A., & Jones, J. C. (2017). Labeling extracellular vesicles for nanoscale flow cytometry. *Scientific Reports*, *7*(1). https://doi.org/10.1038/s41598-017-01731-2

Morikawa, S., Sato, A., & Ezaki, T. (2018). A simple, one-step polychromatic staining method for epoxy-embedded semithin tissue sections. *Microscopy (Oxford, England)*, *67*(6), 331–344. https://doi.org/10.1093/jmicro/dfy037

Northcott, J. M., Dean, I. S., Mouw, J. K., & Weaver, V. M. (2018). Feeling stress: The mechanics of cancer progression and aggression. *Frontiers in Cell and Developmental Biology*, *6*(FEB), 1–12. https://doi.org/10.3389/fcell.2018.00017

Palade, G. (1953). Fine structure of blood. *J Appl Physics*, *24*, 1424.

Park, S.-Y., Kwak, C.-Y., Shayman, J. A., & Kim, J. H. (2012). Globoside promotes activation of ERK by interaction with the epidermal growth factor receptor. *Biochimica et Biophysica Acta*, *1820*(7), 1141–1148. https://doi.org/10.1016/j.bbagen.2012.04.008

Peinado, H., Alečković, M., Lavotshkin, S., Matei, I., Costa-Silva, B., Moreno-Bueno, G., Hergueta-Redondo, M., Williams, C., García-Santos, G., Ghajar, C., Nitadori-Hoshino, A., Hoffman, C., Badal, K., Garcia, B. A., Callahan, M. K., Yuan, J., Martins, V. R., Skog, J., Kaplan, R. N., … Lyden, D. (2012). Melanoma exosomes educate bone marrow progenitor cells toward a pro-metastatic phenotype through MET. *Nature Medicine*, *18*(6), 883–891. https://doi.org/10.1038/nm.2753

Pohl, J., Ring, A., & Stremmel, W. (2002). Uptake of long-chain fatty acids in HepG2 cells involves caveolae: Analysis of a novel pathway. *Journal of Lipid Research*, *43*(9), 1390–1399. https://doi.org/10.1194/jlr.M100404-JLR200

Pol, A., Martin, S., Fernández, M. A., Ingelmo-Torres, M., Ferguson, C., Enrich, C., & Parton, R. G. (2005). Cholesterol and fatty acids regulate dynamic caveolin trafficking through the Golgi complex and between the cell surface and lipid bodies. *Molecular Biology of the Cell*, *16*(4), 2091–2105. https://doi.org/10.1091/mbc.e04-08-0737

Prakash, S., Krishna, A., & Sengupta, D. (2021). Caveolin induced membrane curvature and lipid clustering: two sides of the same coin? *Faraday Discussions*, *232*(0), 218–235. https://doi.org/10.1039/d0fd00062k

Sasaki, N., Toyoda, M., & Ishiwata, T. (2021). Gangliosides as Signaling Regulators in Cancer. *International Journal of Molecular Sciences*, *22*(10). https://doi.org/10.3390/ijms22105076

Sinha, B., Köster, D., Ruez, R., Gonnord, P., Bastiani, M., Abankwa, D., Stan, R. V., Butler-Browne, G., Vedie, B., Johannes, L., Morone, N., Parton, R. G., Raposo, G., Sens, P., Lamaze, C., & Nassoy, P. (2011). Cells respond to mechanical stress by rapid disassembly of caveolae. *Cell*, *144*(3), 402–413. https://doi.org/10.1016/j.cell.2010.12.031

Sonnino, S., & Prinetti, A. (2009). Sphingolipids and membrane environments for caveolin. *FEBS Letters*, *583*(4), 597–606. https://doi.org/10.1016/j.febslet.2009.01.007

Suarez-Arnedo, A., Torres Figueroa, F., Clavijo, C., Arbeláez, P., Cruz, J. C., & Muñoz-Camargo, C. (2020). An image J plugin for the high throughput image analysis of in vitro scratch wound healing assays. *PloS One*, *15*(7), e0232565. https://doi.org/10.1371/journal.pone.0232565

Sung, B. H., Ketova, T., Hoshino, D., Zijlstra, A., & Weaver, A. M. (2015). Directional cell movement through tissues is controlled by exosome secretion. *Nature Communications*, *6*(May). https://doi.org/10.1038/ncomms8164

Théry, C., Witwer, K. W., Aikawa, E., Alcaraz, M. J., Anderson, J. D., Andriantsitohaina, R., Antoniou, A., Arab, T., Archer, F., Atkin-Smith, G. K., Ayre, D. C., Bach, J. M., Bachurski, D., Baharvand, H., Balaj, L., Baldacchino, S., Bauer, N. N., Baxter, A. A., Bebawy, M., … Zuba-Surma, E. K. (2018).

Minimal information for studies of extracellular vesicles 2018 (MISEV2018): a position statement of the International Society for Extracellular Vesicles and update of the MISEV2014 guidelines. *Journal of Extracellular Vesicles*, *7*(1). https://doi.org/10.1080/20013078.2018.1535750

Torrino, S., Shen, W.-W., Blouin, C. M., Mani, S. K., Viaris de Lesegno, C., Bost, P., Grassart, A., Köster, D., Valades-Cruz, C. A., Chambon, V., Johannes, L., Pierobon, P., Soumelis, V., Coirault, C., Vassilopoulos, S., & Lamaze, C. (2018). EHD2 is a mechanotransducer connecting caveolae dynamics with gene transcription. *The Journal of Cell Biology*, *217*(12), 4092–4105. https://doi.org/10.1083/jcb.201801122

Urra, H., Torres, V. A., Ortiz, R. J., Lobos, L., Díaz, M. I., Díaz, N., Härtel, S., Leyton, L., & Quest, A. F. G. (2012). Caveolin-1-enhanced motility and focal adhesion turnover require tyrosine-14 but not accumulation to the rear in metastatic cancer cells. *PloS One*, *7*(4), e33085. https://doi.org/10.1371/journal.pone.0033085

Verweij, F. J., Bebelman, M. P., Jimenez, C. R., Garcia-Vallejo, J. J., Janssen, H., Neefjes, J., Knol, J. C., de Goeij-de Haas, R., Piersma, S. R., Baglio, S. R., Verhage, M., Middeldorp, J. M., Zomer, A., van Rheenen, J., Coppolino, M. G., Hurbain, I., Raposo, G., Smit, M. J., Toonen, R. F. G., … Pegtel, D. M. (2018). Quantifying exosome secretion from single cells reveals a modulatory role for GPCR signaling. *Journal of Cell Biology*, *217*(3), 1129–1142. https://doi.org/10.1083/jcb.201703206

Wang, K., Zhu, X., Mei, D., & Ding, Z. (2018). Caveolin-1 contributes to anoikis resistance in human gastric cancer SGC-7901 cells via regulating Src-

dependent EGFR-ITGB1 signaling. *Journal of Biochemical and Molecular Toxicology*, *32*(10), e22202. https://doi.org/10.1002/jbt.22202

Wu, Y., Deng, W., & Klinke, D. J. 2nd. (2015). Exosomes: improved methods to characterize their morphology, RNA content, and surface protein biomarkers. *The Analyst*, *140*(19), 6631–6642. https://doi.org/10.1039/c5an00688k

Yáñez-Mó, M., Siljander, P. R. M., Andreu, Z., Zavec, A. B., Borràs, F. E., Buzas, E. I., Buzas, K., Casal, E., Cappello, F., Carvalho, J., Colás, E., Cordeiro-Da Silva, A., Fais, S., Falcon-Perez, J. M., Ghobrial, I. M., Giebel, B., Gimona, M., Graner, M., Gursel, I., … De Wever, O. (2015). Biological properties of extracellular vesicles and their physiological functions. *Journal of Extracellular Vesicles*, *4*(2015), 1–60. https://doi.org/10.3402/jev.v4.27066

Figure 1: Characterization of EVs from mechanically stressed cells.

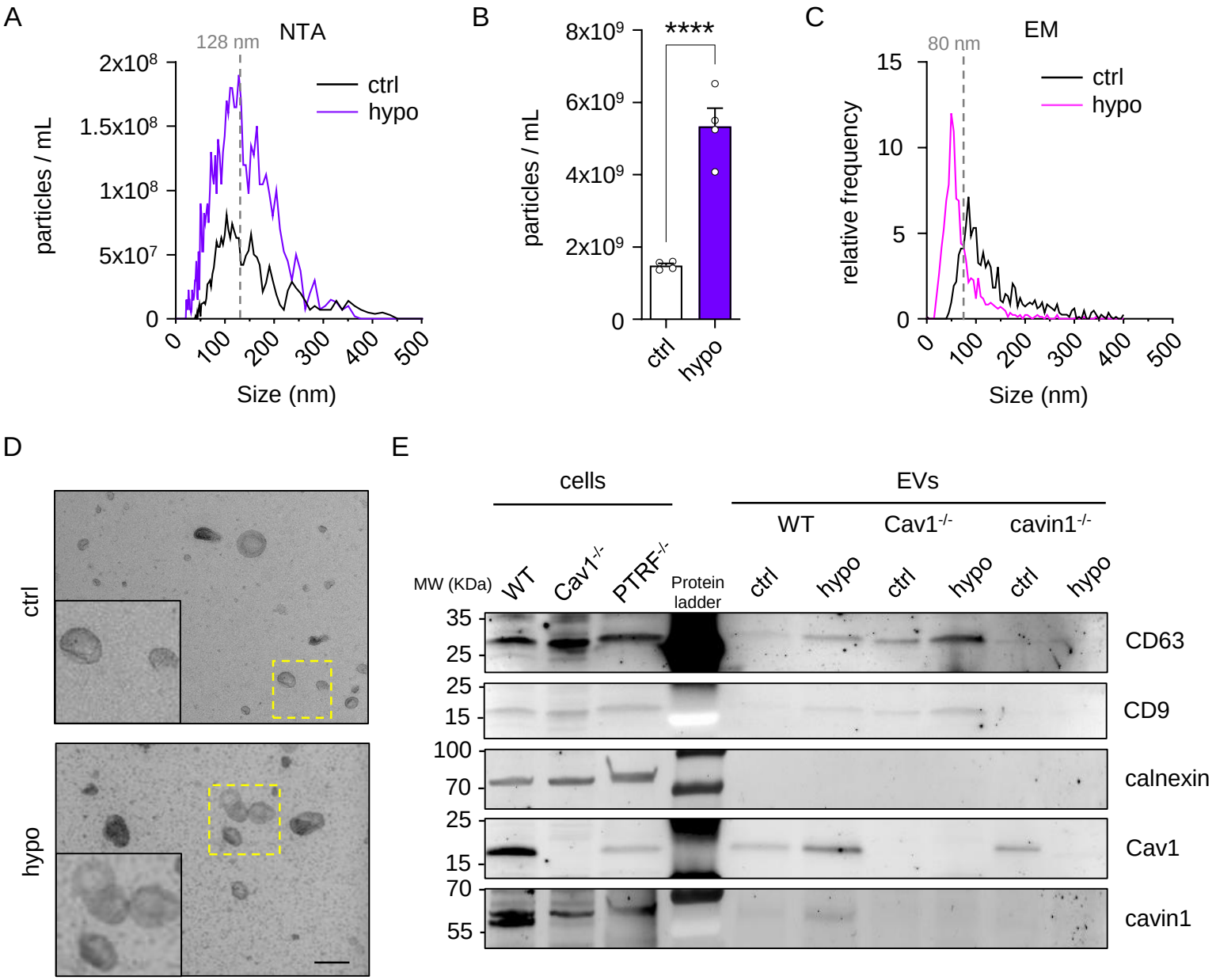

Figure 2: Mechanical stress effects on EV release.

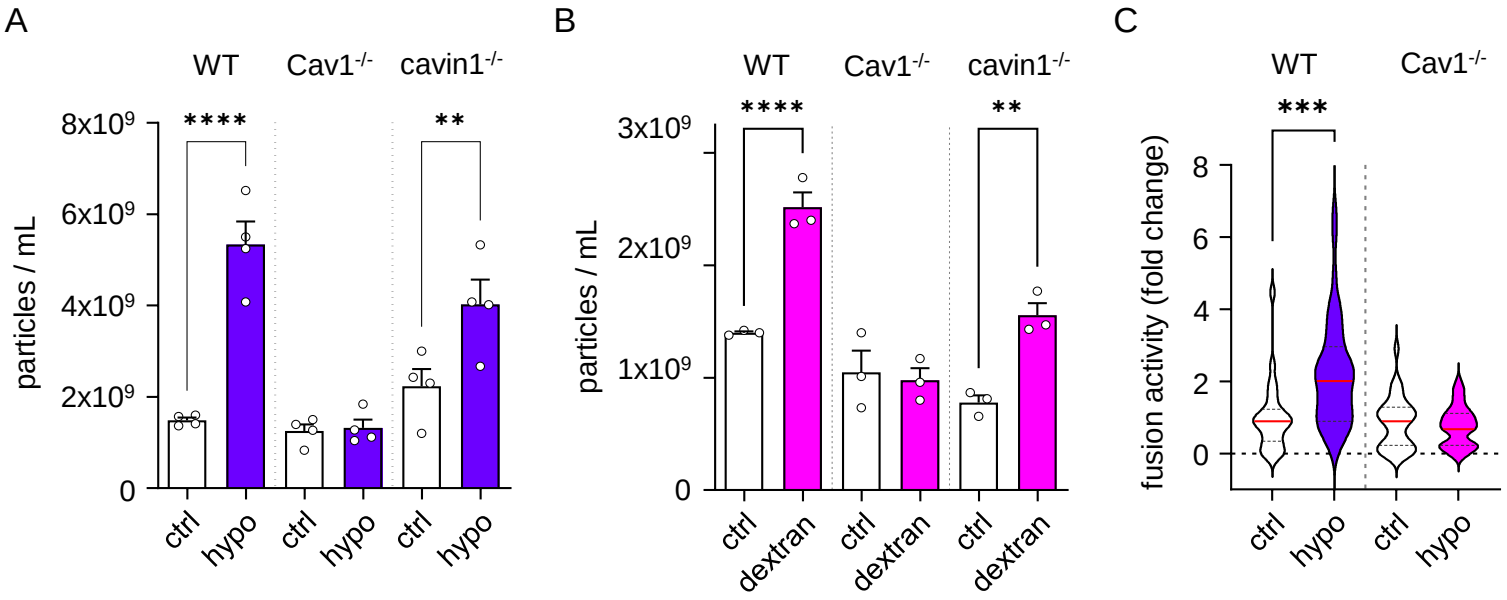

Figure 3: Impact of mechanical stress on MVBs.

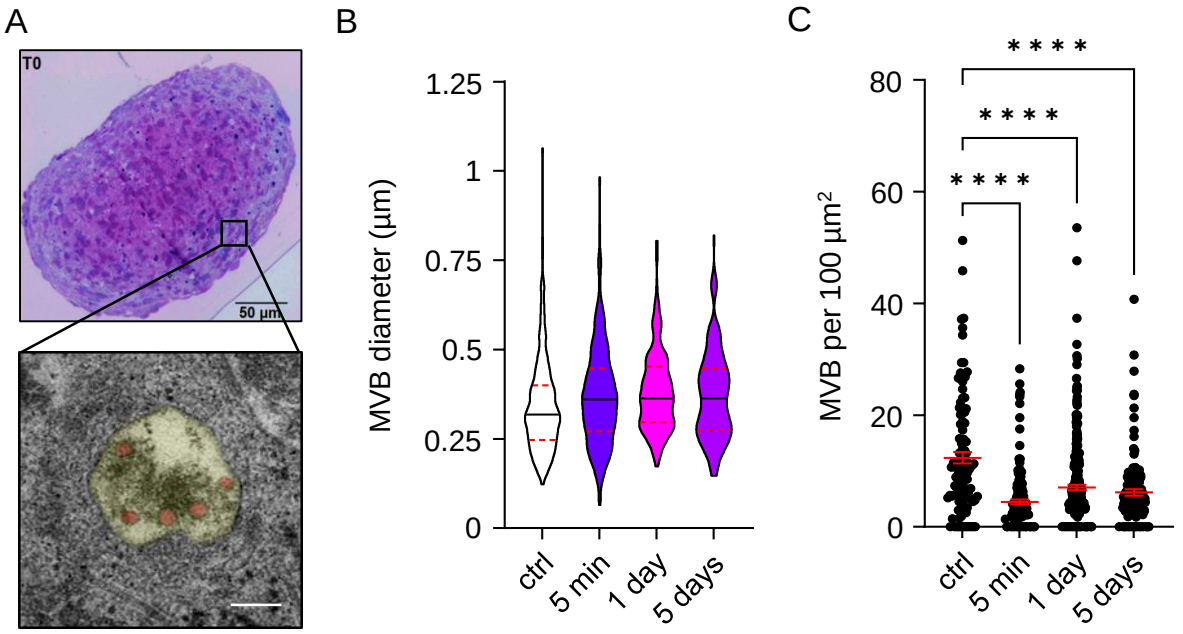

Figure 4: Analysis of the ESCRT pathway in EV release.

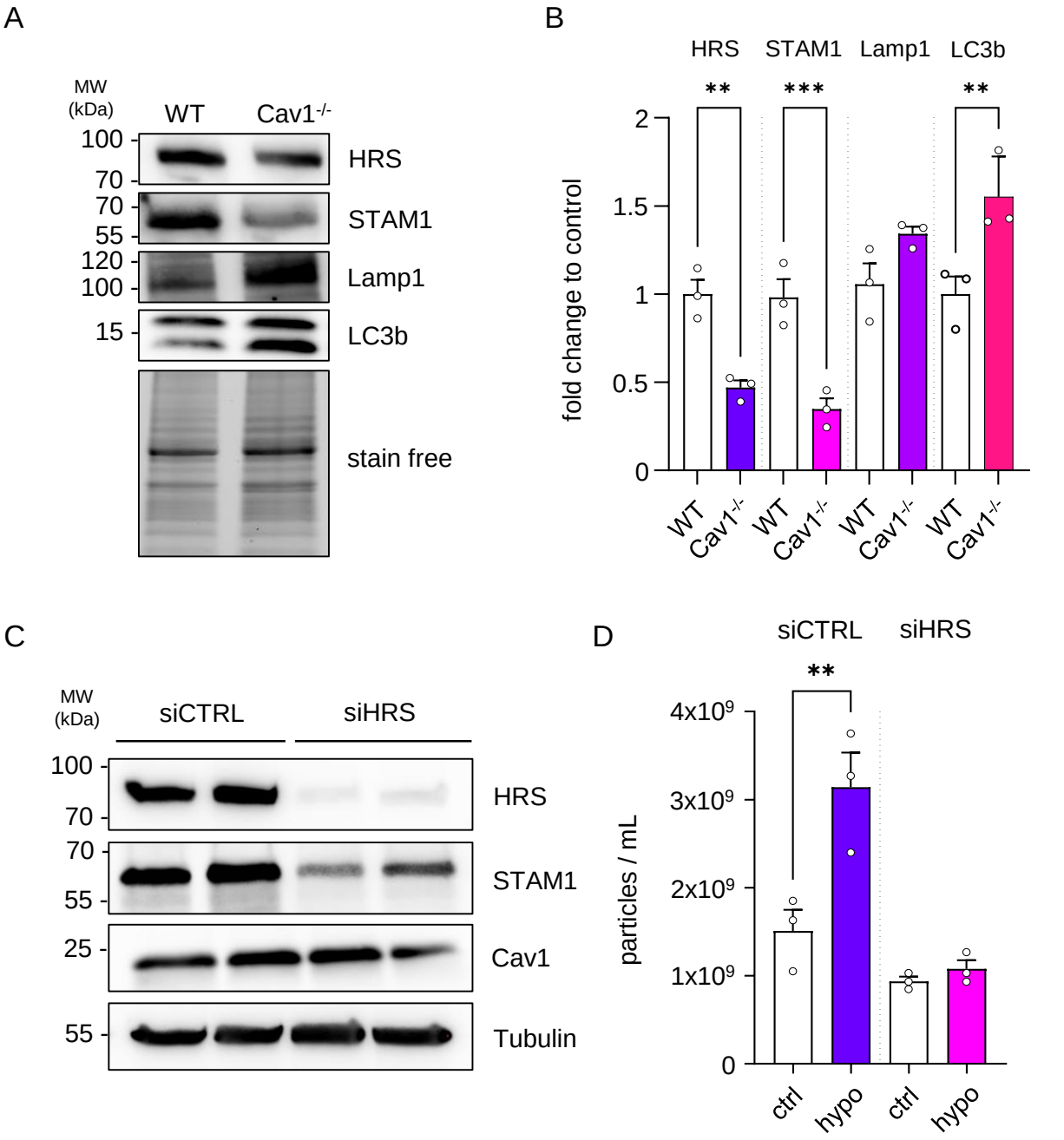

Figure 5: Lipid signature of EVs from mechanically stressed cells.

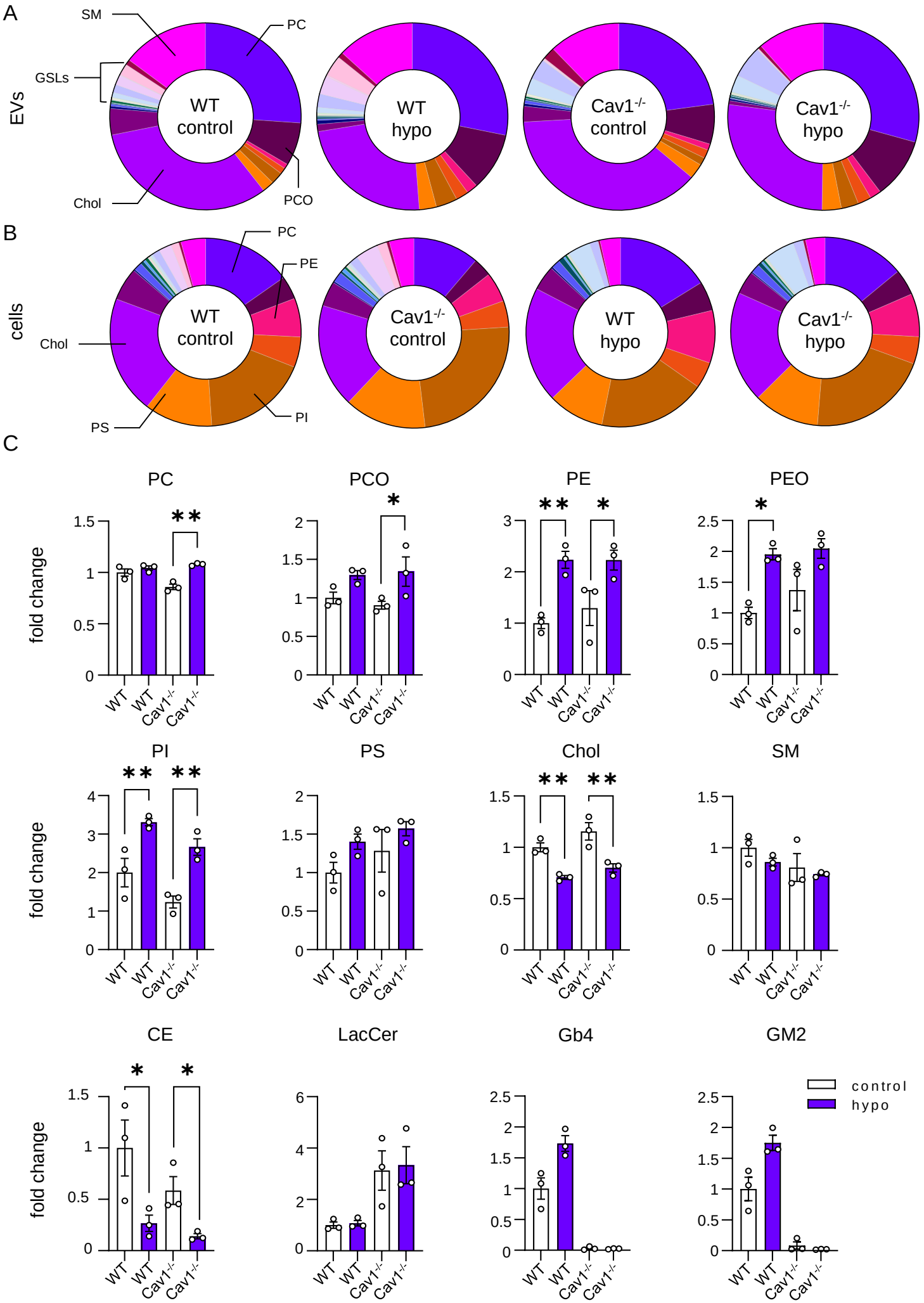

Figure 6: Protein signature of EVs from mechanically stressed cells.

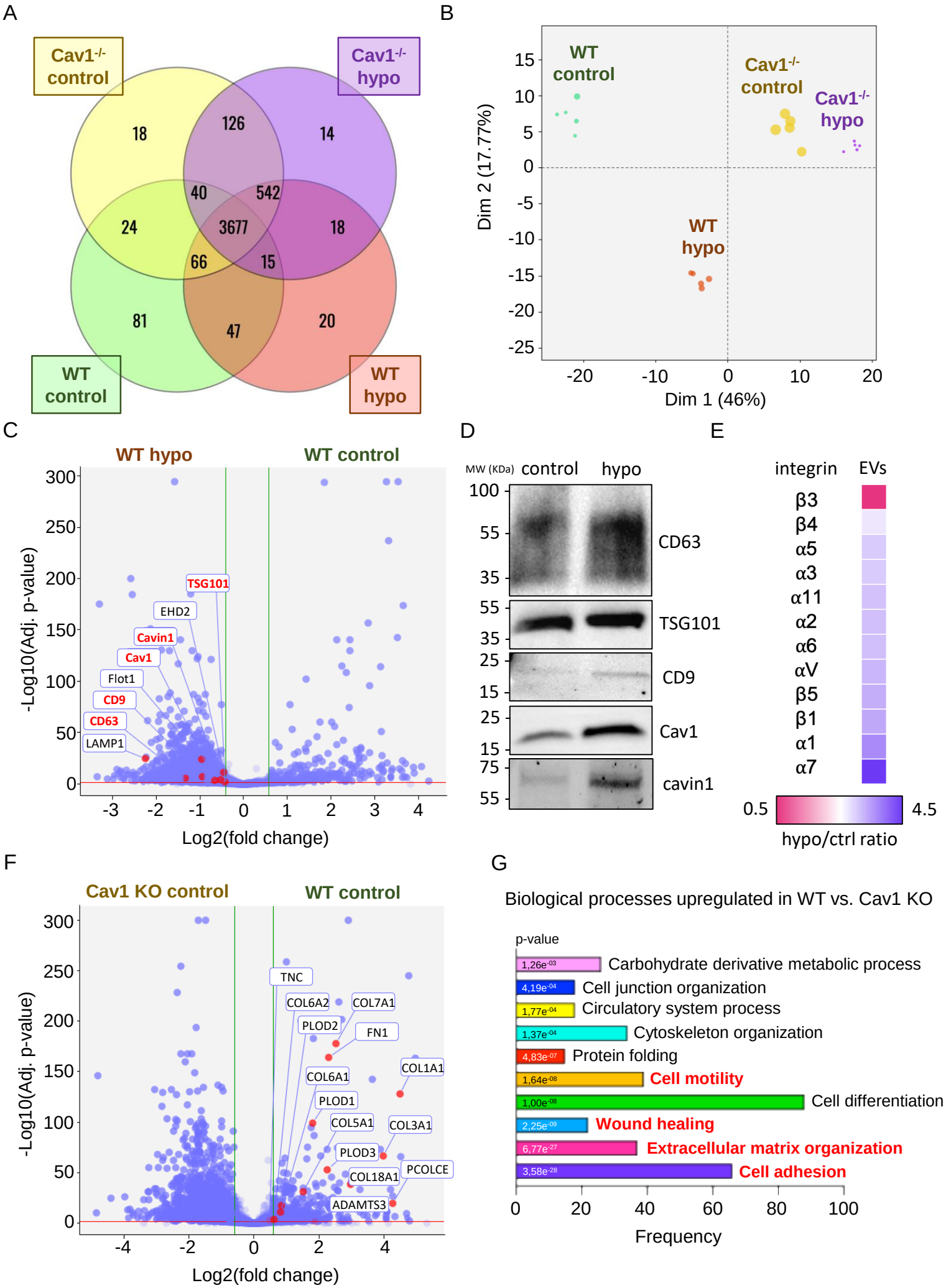

Figure 7: Migration and invasion of Hs578t cells treated with EVs.

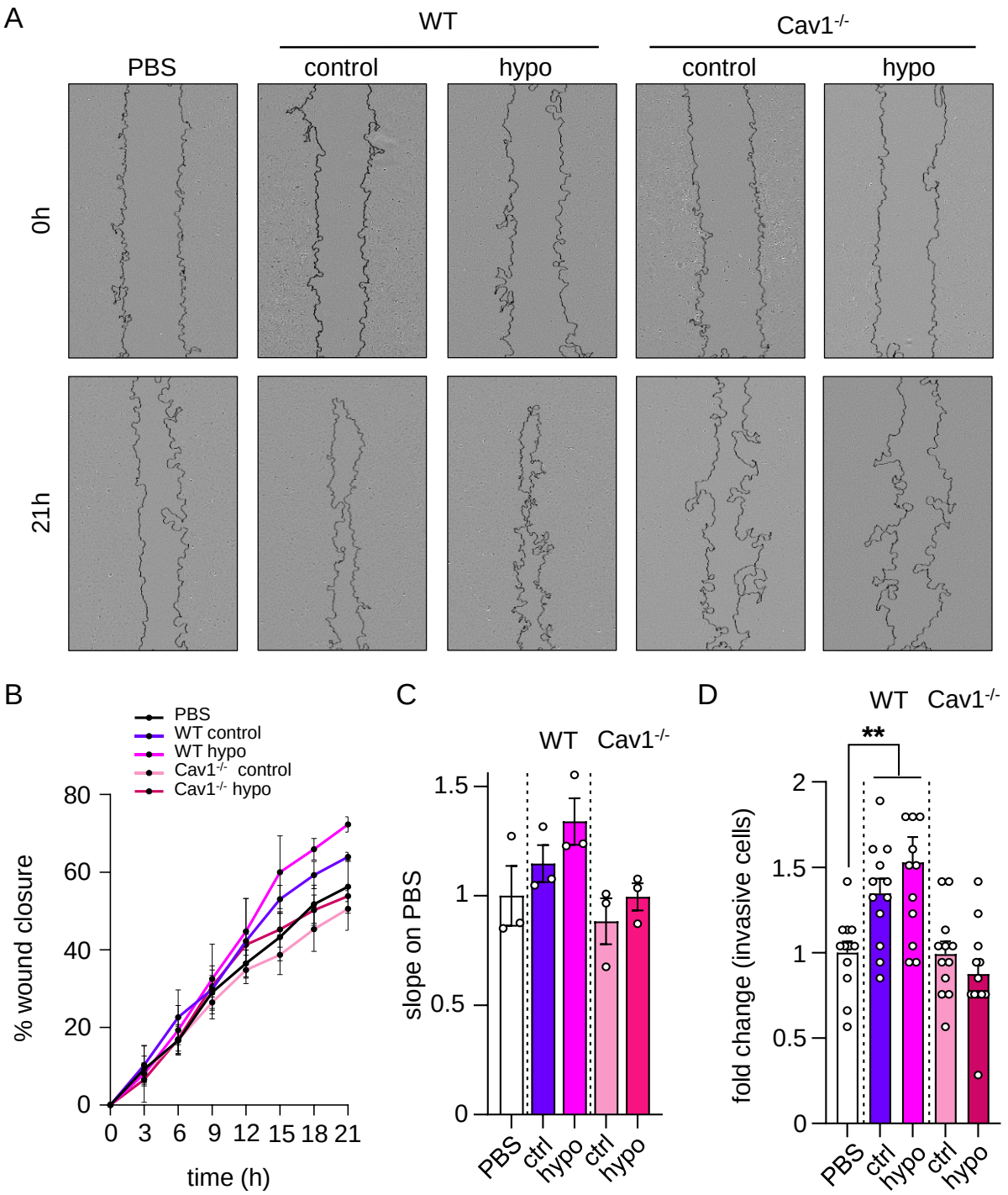

Supplementary figure 1: Validation of mechanical stress models.

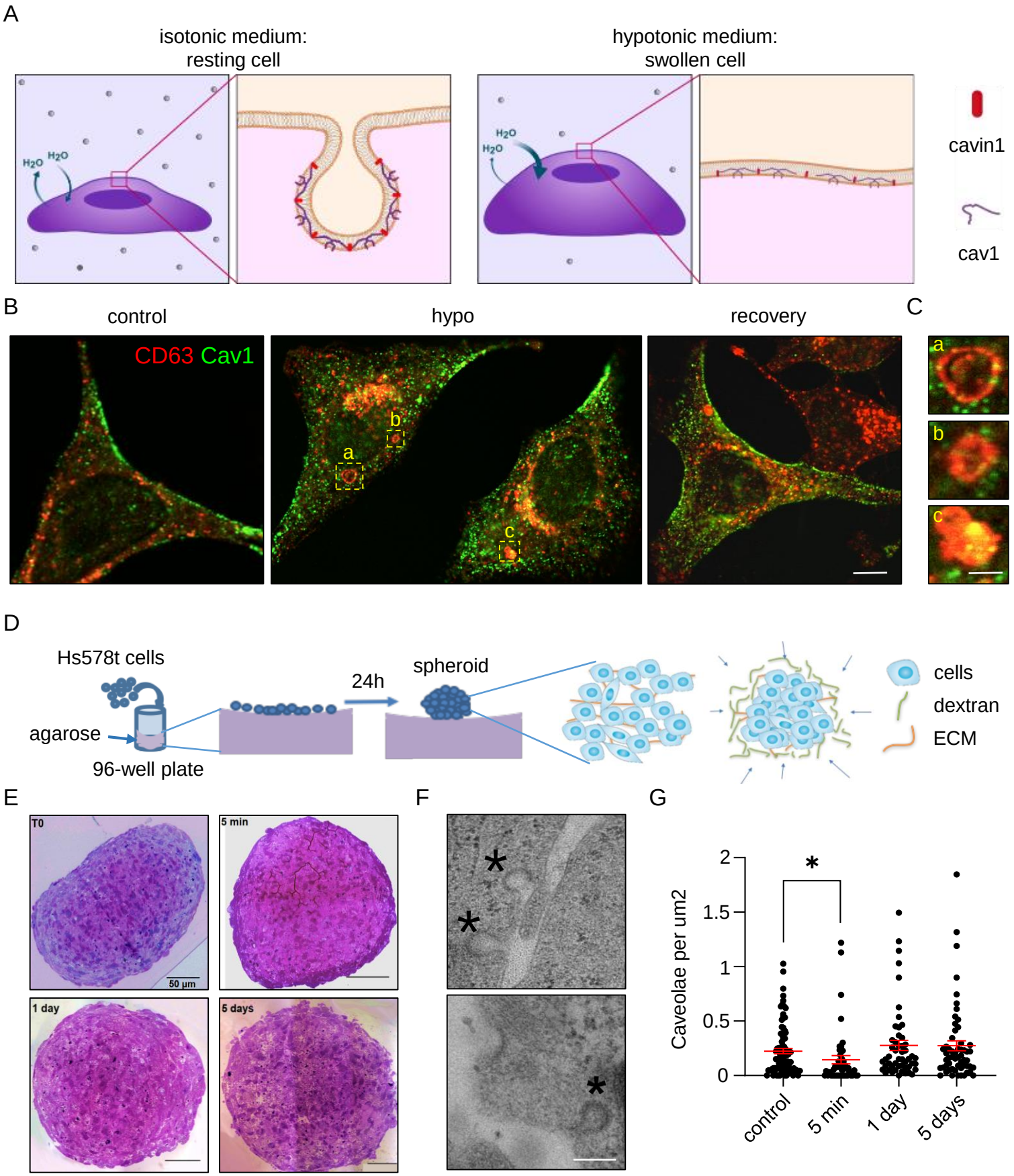

Supplementary figure 2: Effect of mechanical stress on EV secretion in additional cell lines.

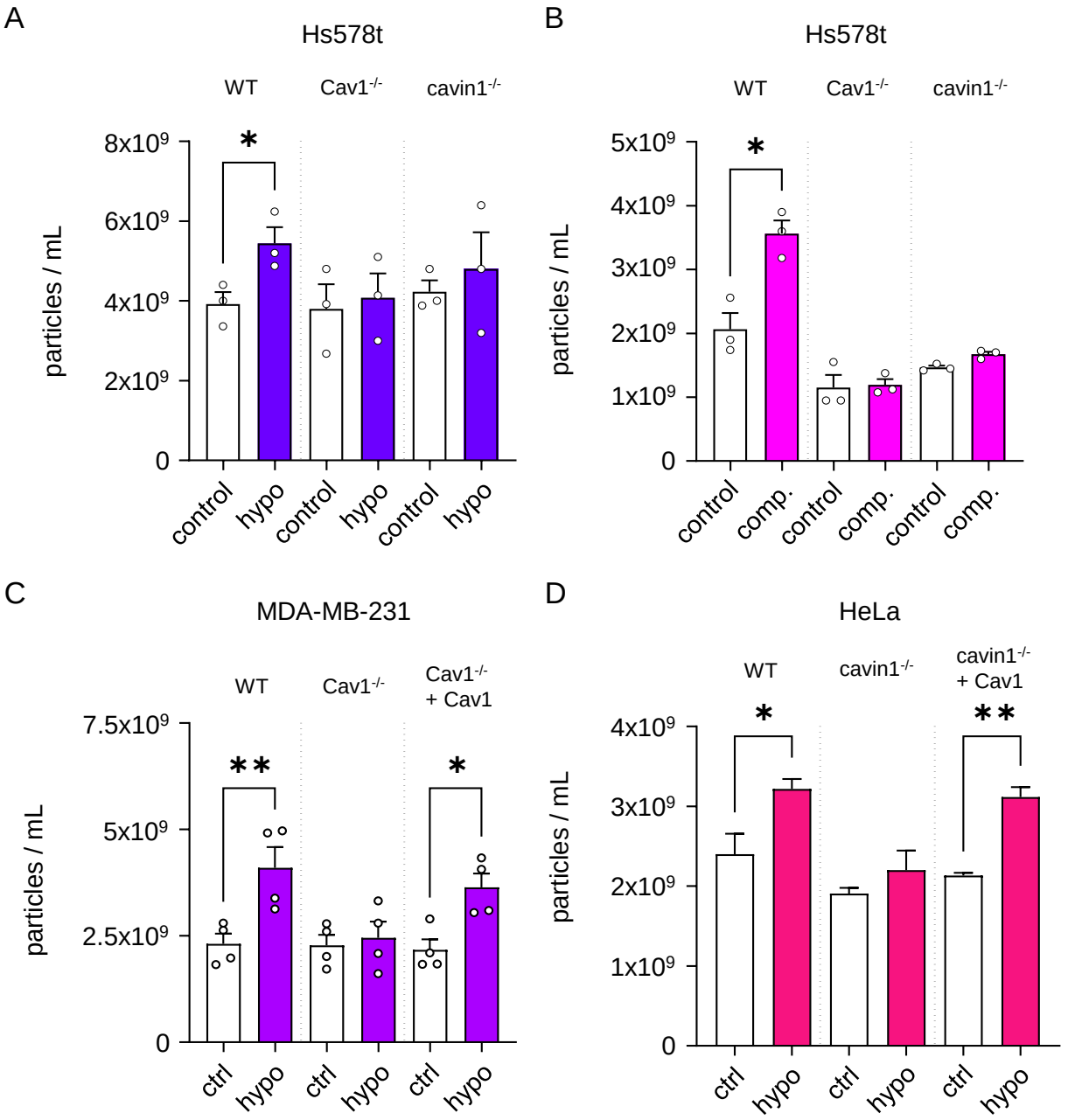

Supplementary figure 3: EV uptake by Hs578t cells.

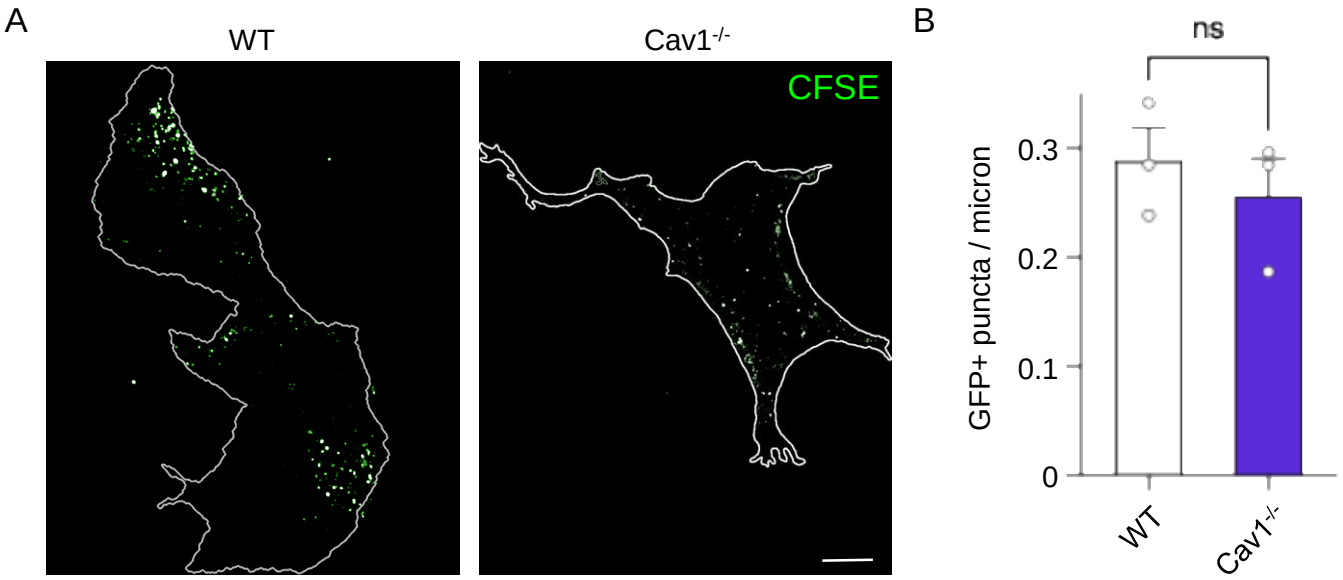
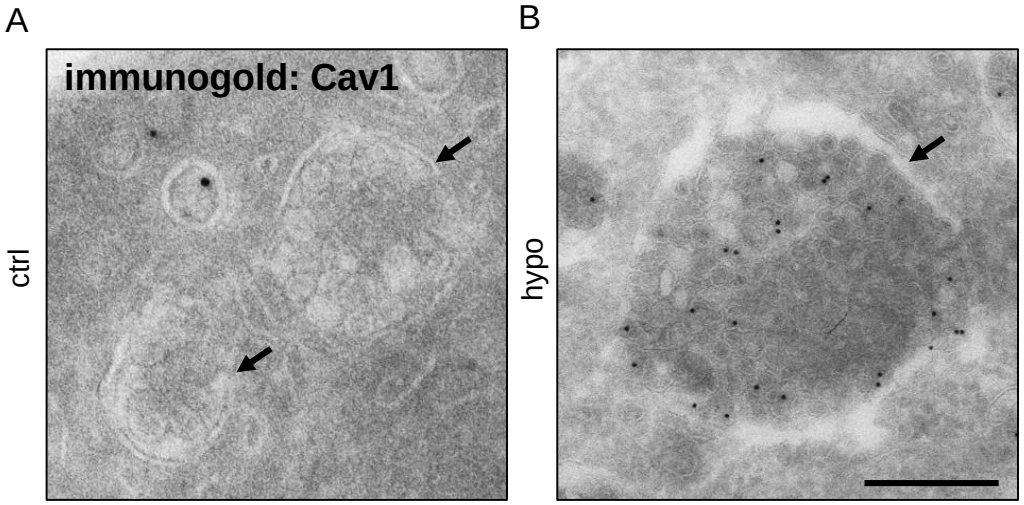
Supplementary figure 4: Cav1 localization at MVBs after mechanical stress.